

CHEMISTRY

Corner-, edge-, and facet-controlled growth of nanocrystals

Yuanwei Li^{1,2*}, Haixin Lin^{2,3*}, Wenjie Zhou^{2,3*}, Lin Sun^{2,4},
Devleena Samanta^{2,3}, Chad A. Mirkin^{1,2,3,4†}

The ability to precisely control nanocrystal (NC) shape and composition is useful in many fields, including catalysis and plasmonics. Seed-mediated strategies have proven effective for preparing a wide variety of structures, but a poor understanding of how to selectively grow corners, edges, and facets has limited the development of a general strategy to control structure evolution. Here, we report a universal synthetic strategy for directing the site-specific growth of anisotropic seeds to prepare a library of designer nanostructures. This strategy leverages nucleation energy barrier profiles and the chemical potential of the growth solution to control the site-specific growth of NCs into exotic shapes and compositions. This strategy can be used to not only control where growth occurs on anisotropic seeds but also control the exposed facets of the newly grown regions. NCs of many shapes are synthesized, including over 10 here-to-fore never reported NCs and, in principle, many others are possible.

INTRODUCTION

Nanocrystal (NC) shape and composition are important parameters that influence the properties of such structures and, therefore, their uses in many fields, including catalysis (1–3), plasmonics (4, 5), therapeutics (6), and biological imaging (6, 7). Accordingly, a variety of methods have been developed that allow one to control these parameters, albeit in selected cases (8–11). The most prevalent methodologies involve seed-mediated syntheses. For example, capping agents have been used to selectively cap different faces of spherical seeds to promote anisotropic growth and the formation of nanocubes, octahedra, rhombic dodecahedra, and NCs of other shapes (12–15). Spherical gold and silver NCs have been used as plasmonic seeds, where light of a specific wavelength was used to guide the growth of triangular prisms with wavelength control over prism edge length (16, 17). In addition, underpotential deposition techniques have been used with gold and palladium seeds to prepare a wide variety of NC geometries, including rhombic dodecahedra, bipyramids, truncated ditetragonal prisms, and concave cubes (18–21).

While most studies have focused on spherical seeds, some anisotropic seeds have been used to prepare a variety of structures. For example, rod-shaped seeds have been used to generate elongated rhombic dodecahedral gold NCs (22). Moreover, rhombic dodecahedral gold seeds have been used as cores for the synthesis of Au-Ag core-shell NCs with cubic, cuboctahedral, and octahedral structures (23). Anisotropic seeds combined with masking or galvanic replacement have been used to prepare heterogeneous metallic or hollow nanostructures (24–26).

However, with most traditional seed-mediated approaches, the spherical or anisotropic seeds act as nuclei due to the absence of substantial energy barriers (E) for subsequent growth. Consequently, secondary nucleation does not occur, and instead, growth occurs at all positions on the seeds. Therefore, the development of a versatile

strategy that allows one to control growth on seeds in a site-specific manner is a challenge yet to be addressed.

We reasoned that if we could introduce distinct E for secondary nucleation at different sites on an anisotropic seed, we would be able to achieve site-specific deposition by controlling the sites of secondary nucleation. If one analyzes the surface chemistry of a nonspherical seed, such as a triangular prism, one discovers that there are distinct E to additional growth due to differences in ligand density (caused by regions of different curvature; i.e., flat facets versus edges versus corners) and the exposed facet type (27–29). Therefore, we hypothesized that, through the use of appropriate ligands, substantial E differences on anisotropic seeds could be established, allowing one to access corner-, edge-, or facet-selective growth while tuning the supersaturation ($\Delta\mu$) of the growth solution (the driving force) to only surmount certain E . In addition, further fine-tuning of $\Delta\mu$ would not only dictate the site of deposition (e.g., the edge or corner of an octahedron) but also determine the exposed facets (e.g., {100} or {111}) of the overgrown regions, thus controlling the overall shapes of the resulting NCs. Therefore, the ability to selectively grow additional material at specific sites on anisotropic seeds could be a general route for preparing a library of designer architectures with different shapes and compositions by following three fundamental design rules (curvature-selective, facet-selective, and specific exposed facet design rules).

RESULTS

The driving force for NC growth is the $\Delta\mu$ of the growth solution, which can be defined as the difference between chemical potential of the solute in solution (e.g., Au⁰ atoms) and that of the solid crystal (e.g., Au seed) (30). Growth only occurs at sites on anisotropic seeds when $\Delta\mu$ can surmount the nucleation E (i.e., $\Delta\mu > E$). The E can be influenced by two factors—the curvature-dependent ligand distribution and the facet-dependent energy differences. We discuss below how $\Delta\mu$ and E can be independently tuned leading to site-specific nucleation and growth.

Curvature-selective design rule: Sites with larger curvatures grow at lower $\Delta\mu$

Ligands tethered onto regions of different curvature on an anisotropic NC experience different degrees of confinement (28, 31), which

Copyright © 2021
The Authors, some
rights reserved;
exclusive licensee
American Association
for the Advancement
of Science. No claim to
original U.S. Government
Works. Distributed
under a Creative
Commons Attribution
NonCommercial
License 4.0 (CC BY-NC).

¹Department of Chemical and Biological Engineering, Northwestern University, Evanston, IL 60208, USA. ²International Institute for Nanotechnology, Northwestern University, Evanston, IL 60208, USA. ³Department of Chemistry, Northwestern University, Evanston, IL 60208, USA. ⁴Department of Materials Science and Engineering, Northwestern University, Evanston, IL 60208, USA.

*These authors contributed equally to this work.

†Corresponding author. Email: chadnano@northwestern.edu

ultimately translates into varying magnitudes of E at different sites. For example, triangular gold nanoprisms with different curvatures at corners (c), edges (e), and faces (f) are an excellent model system to investigate this premise. As shown in Fig. 1 (A to C), when the curvature (K) at a site is higher, the average distance between the ligands (δ) is larger ($K_c > K_e > K_f$ such that $\delta_c > \delta_e > \delta_f$), which provides easier access to solutes for subsequent deposition and results in a lower E for that site ($E_c < E_e < E_f$). Therefore, by adjusting the $\Delta\mu$ of the growth solution, specific curvature-selective energy windows can be attained, enabling corner- and edge-selective nucleation (Fig. 1A). Experimentally, we can tune $\Delta\mu$ of the growth solution by changing the reaction conditions. For example, increasing the concentration of the reducing agent ascorbic acid (AA), decreasing the reduction potential of the reduction agent, or decreasing the concentration of the ligand adsorbate hexadecyltrimethylammonium bromide (CTAB) all result in increased $\Delta\mu$ (detailed discussion in the Supplementary Materials).

To achieve selective growth, E_c , E_e , and E_f must be well separated in magnitude. The length and binding affinity of the ligands are key parameters that affect the E profiles and growth selectivity (see the Supplementary Materials for additional discussion). When a weakly binding ligand is used (e.g., CTAB), the E values and their differences are negligible, resulting in uniform growth of the nanoprism into a larger nanoprism (fig. S2). In other words, when only CTAB is used, secondary nucleation does not occur and growth selectivity cannot be achieved. We further studied ligands with higher binding affinities that can displace CTAB, including mPEG5k thiol and mPEG6 disulfide, such that CTAB in the following study is used only as a complexing agent to tune $\Delta\mu$ not E (see note S1 for additional discussion) (32). However, when a relatively long ligand with a high binding affinity is used (e.g., mPEG5k thiol), the E values of the nanoprisms exceed the homogeneous nucleation E , and growth is not observed on the nanoprisms even when $\Delta\mu$ is higher than homogeneous nucleation E (fig. S2). We empirically found that mPEG6 disulfide results in the desired E profiles, such that the $\Delta\mu$ - E relationship can be tuned to achieve corner-selective ($E_c < \Delta\mu < E_e$) and edge-

selective ($E_e < \Delta\mu < E_f$) nucleation (Fig. 1D). Therefore, this ligand is used in all subsequent studies. Together, the curvature-selective design rule is that sites with larger K grow at lower $\Delta\mu$.

To test the generality of this curvature-selective design rule, NCs of various polyhedral shapes are used as seeds. Octahedral and concave rhombic dodecahedral gold seeds (Fig. 2, A and B) have corners and edges with different curvatures. Regardless of the polyhedral geometry of the seeds, subsequent site-specific gold deposition only on the corners (Fig. 2, D and E) or only the edges (Fig. 2, H and I) can be obtained by changing the AA concentration to tune the $\Delta\mu$ relative to E . When a seed NC has multiple types of corners (or edges) that are energetically nonequivalent, $\Delta\mu$ can be further tuned so that nucleation occurs preferentially at the lower- E sites first. For example, in case of decahedral gold seeds (Fig. 2C) with two types of corners (a and b) and two types of edges (c and d) ($K_a > K_b > K_c > K_d$), four levels of continuous but independent control are possible over the selective growth on the different corners (Fig. 2, F and G) and edges (Fig. 2, J and K). Namely, we can successively grow (i) site a; (ii) sites a and b; (iii) sites a, b, and c; and (iv) sites a, b, c, and d.

Facet-selective design rule: Facets with higher surface energies grow at lower $\Delta\mu$

In addition to the curvature differences, facet energy (σ) differences also play an important role in influencing the corresponding E profiles for subsequent NC nucleation. To decouple the effects of differing facets from that of curvature, the side faces of nanorods with no curvature difference, which are bound by alternating {100} and {110} facets (33), are used as a model system. The higher the σ (resulting from the lower coordination number), the lower the E (see the Supplementary Materials for detailed discussion) and the easier it is for solutes to access sites for subsequent nucleation. Therefore, by adjusting the $\Delta\mu$ - E relationship, specific facet-selective nucleation windows can be reached (Fig. 3A). Specifically, $\sigma_{\{110\}} > \sigma_{\{100\}}$ such that

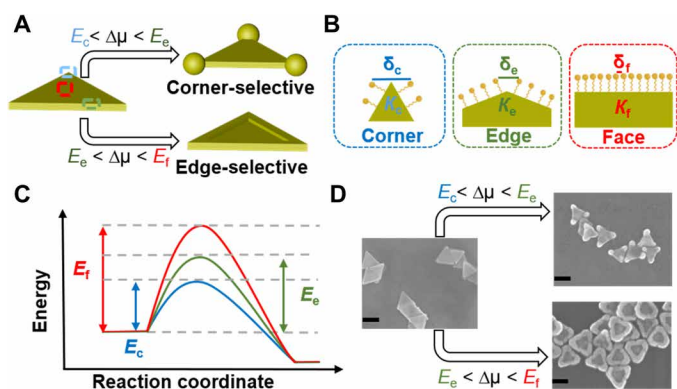


Fig. 1. Curvature-selective nucleation on a seed NC. (A) The $\Delta\mu$ for NC growth can be tuned to favor corner- and edge-selective growth. (B) Pictures depicting different regions [corners (c), edges (e), and faces (f)] of a Au nanoprism with varying curvatures and, therefore, different ligand distributions. The higher the curvature (K), the larger the average distance between the ligands (δ) (here, $K_c > K_e > K_f$ such that $\delta_c > \delta_e > \delta_f$). (C) Schematic showing the general trend of the E profile for NC growth, which is dictated by the degree of curvature, to illustrate the relationship $E_c < E_e < E_f$. (D) Scanning electron microscopy (SEM) images showing corner- and edge-selective nucleation on Au nanoprisms. Scale bars, 100 nm.

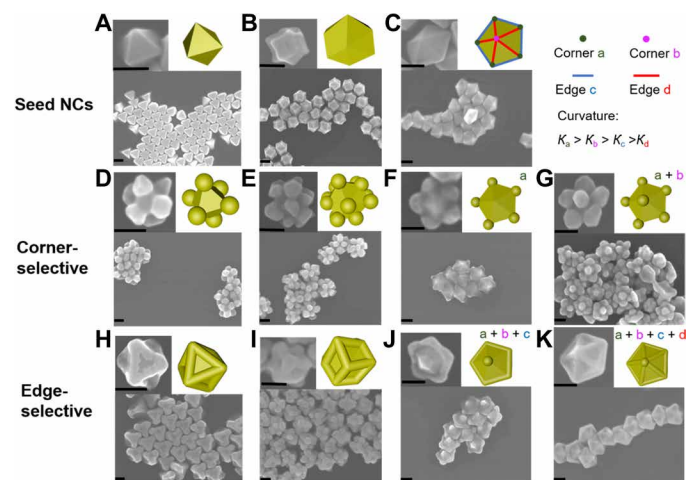


Fig. 2. Curvature-selective nucleation on different-shaped seed NCs. (A to C) SEM images and models (inset top right) of octahedral, concave rhombic dodecahedral, and decahedral Au seed NCs, respectively. SEM images and models (inset top right) of (D to G) corner- and (H to K) edge-selective nucleation on the seed NC shown in the top row. Decahedral NCs (C) contain two types of corners (a and b) and two types of edges (c and d) due to curvature differences such that $K_a > K_b > K_c > K_d$, which results in four levels of continuous but independent control of selective nucleation as seen in (F), (G), (J), and (K). Scale bars, 100 nm.

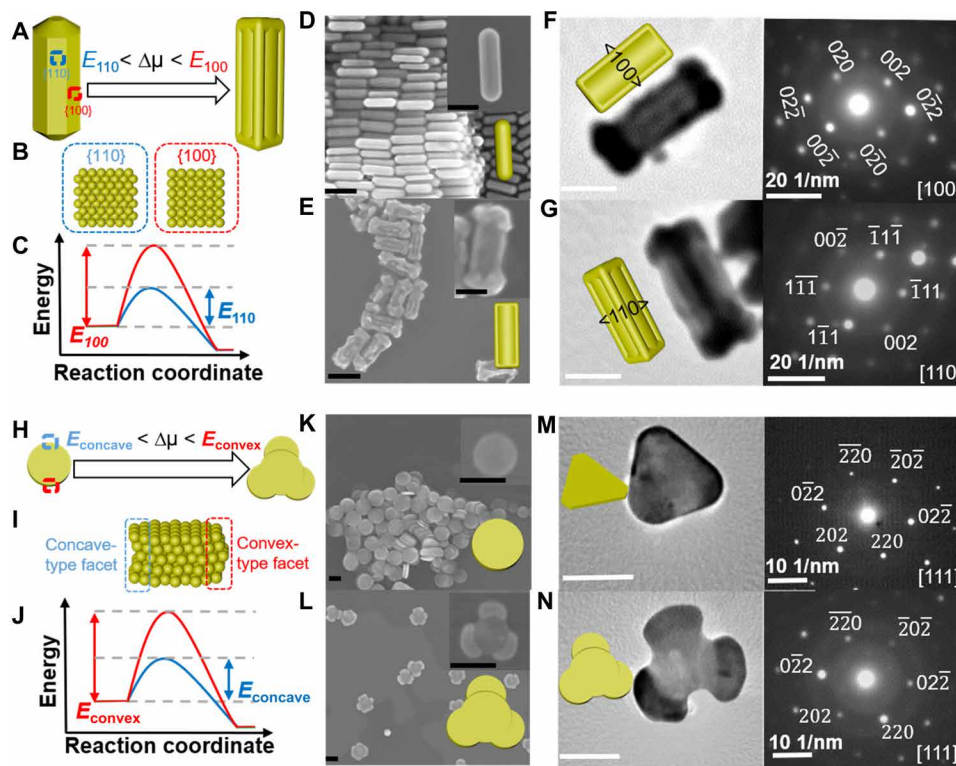


Fig. 3. Facet-selective nucleation on the edges. (A) Schematic of facet-selective growth on a Au nanorod, where growth can occur on (B) only the {110} facets of the seed NC by tuning $\Delta\mu$. (C) The idealized E profile for NC growth is dictated by the facet's energy, where $E_{\{110\}} < E_{\{100\}}$. SEM images of (D) Au nanorods and (E) {110} facet-selective growth on nanorods. Transmission electron microscopy (TEM) images and corresponding SAED patterns of nanorods with {110} facet-selective growth oriented along the (F) [100] and (G) [110] directions. (H) Schematic of concave-type facet-selective nucleation on Au nanodisks, where the concave-type facet-selective window can be reached by tuning $\Delta\mu$. (I) Side view of a Au nanodisk showing the concave- and convex-type facets. (J) Schematic showing the general trend of the E profile of Au nanodisks, where $E_{\text{concave}} < E_{\text{convex}}$. SEM images of (K) Au nanodisks and (L) facet-selective grown nanodisks. TEM images and corresponding SAED patterns of (M) a Au nanoprism and (N) a Au nanodisk after concave-type facet-selective growth. The diffraction patterns in (M) and (N) are diagnostic of the [111] orientation. Scale bars, 100 nm.

$E_{\{110\}} < E_{\{100\}}$ (Fig. 3, B and C). Therefore, subsequent gold atoms were only selectively deposited on the four {110} facets of the nanorods' side faces when $\Delta\mu$ only surmounts $E_{\{110\}}$ (Fig. 3, D and E). The selected area electron diffraction (SAED) patterns (Fig. 3, F and G) show that the newly grown parts are in the direction of the $\langle 110 \rangle$ zone axis of the nanorods, while the parts in the orientation of the $\langle 100 \rangle$ zone axis did not grow, thus confirming {110} facet-selective nucleation and growth. Together, the facet-selective design rule that emerges from this study is that facets with higher σ grow at lower $\Delta\mu$.

The facet-selective design rule can also be generally applied to predict and tailor nanostructures when gold nanodisks are used as seeds (Fig. 3H). Gold nanodisks are synthesized by etching triangular nanoprisms, and the three areas of these nanodisks that used to be the prism corners have the same atomic arrangement as that of the original nanoprism corners. Along the edges of the nanodisks, the stacking fault of the twin plane causes {111} faces to form in alternating concave or convex orientations (Fig. 3I) (34). The concave structure creates a reentrant groove, a self-perpetuating ledge that increases the number of nearest neighbors for an adatom, increasing the stabilization energy, and greatly decreasing E_{concave} . However, on the convex side, an adatom attached to the surface has limited stabilization energy due to the presence of only three nearest neighbors, resulting in a higher E_{convex} (Fig. 3J). Therefore, deposition occurs exclusively on the concave-type facets when $E_{\text{concave}} < \Delta\mu < E_{\text{convex}}$

(Fig. 3L). SAED patterns (Fig. 3, M and N) indicate that the edges are grown in the same directions as the three original corners of the nanoprisms, thus suggesting concave-type facet-selective nucleation. Therefore, facet-selective nucleation that is not accessible using existing synthetic strategies can be achieved by taking advantage of facet-dependent energy differences coupled with E profiles, which may provide an opportunity to design materials that could offer previously unknown fundamental insights and previously inaccessible functionalities.

Specific exposed facet design rule: Facets with higher surface energies are exposed at higher $\Delta\mu$

In addition to spatial control over nucleation, the $\Delta\mu$ - E relationship can be further tuned to control the exposed facets of the growth on the existing nuclei, thus programming the resulting shapes of the NCs. On the basis of the Thomson-Gibbs equation (32) in a growing crystal, facets with higher surface energies will appear when the $\Delta\mu$ of the growth solution is higher (detailed discussion in the Supplementary Materials). For example, in the case of gold nanocubes and octahedra, the surface energy of {100} in dark green is higher than that of {111} in light green (Fig. 4A). Therefore, using corner-nucleated octahedra as seeds (Fig. 4, B and E), growth occurs almost exclusively on the existing nuclei on the corners. The corners are bound by {111} facets at lower $\Delta\mu$ (100 mM CTAB) (Fig. 4, B and F), while the {100} facets begin to appear on the corners at higher $\Delta\mu$

(10 mM CTAB) (Fig. 4, B and G). Moreover, when edge-nucleated nanocubes are used as seeds (Fig. 4, C and I), subsequent growth only occurs on the existing nuclei along the edges. The edges are bound by {100} facets at higher $\Delta\mu$ (10 mM CTAB) (Fig. 4, C and J),

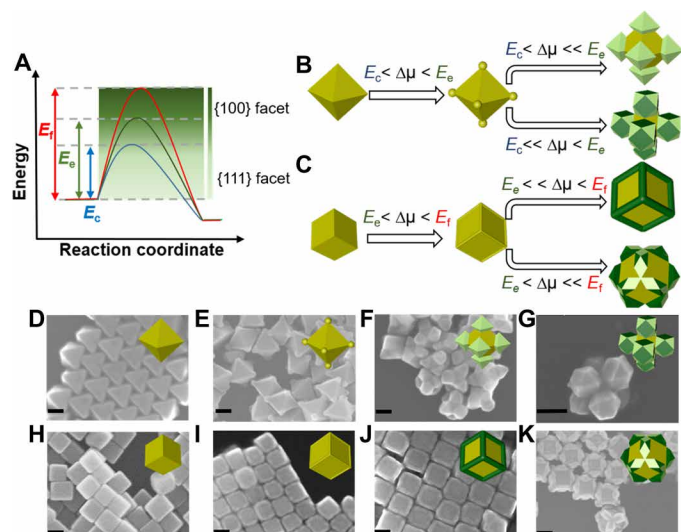


Fig. 4. Tuning the chemical potential of the growth solution controls the exposed facets. (A) Schematic showing the general trend of the E profile of NCs. Different facets are favored on the basis of differences in facet surface energies [{100} facets (dark green) have higher energy than {111} facets (light green)]. Using (B) corner-nucleated Au octahedra or (C) edge-nucleated Au nanocubes as seeds, the facets of the NCs grown on the existing nuclei on the corners of octahedra or along the edges of the nanocubes can be tuned through fine control of $\Delta\mu$. SEM images of (D) Au octahedra, (E) corner-nucleated octahedra, and octahedra after corner-selective growth with (F) {111} and (G) {100} and {111} facets exposed. SEM images of (H) Au nanocubes, (I) edge-nucleated nanocubes, and nanocubes after edge-selective growth with (J) {100} and (K) {100} and {111} facets exposed. Scale bars, 100 nm.

while the {111} facets begin to appear along the edges at lower $\Delta\mu$ (100 mM CTAB) (Fig. 4, C and K, and fig. S8).

Furthermore, a broad library of structures with specific exposed facets can be obtained by controlling the concentration of the seeds in addition to $\Delta\mu$ (figs. S9 and S10). This exposed facet design rule can be applied to seeds of different shapes, such as gold concave rhombic dodecahedra and nanodisks (fig. S10, see the Supplementary Materials for a detailed discussion). These results not only confirm the design rule but also markedly increase the number and diversity of nanostructures that can be accessed using seed-mediated syntheses.

General use of this strategy

To further explore the generality of this strategy, gold NC seed growth was studied as a function of growth solution metal ion composition and reducing agent. Corner- or edge-selective growth of Ag or Pd onto Au NCs of different shapes, including nanoprisms, octahedra, and concave rhombic dodecahedra, can be similarly controlled (Fig. 5). Elemental mapping confirms the spatial arrangement of the NCs. Therefore, this strategy provides a way to expand the compositional library of NCs through crystal engineering via site-specific growth.

DISCUSSION

We have developed a new and versatile synthetic strategy, where curvature/facet-dependent E and $\Delta\mu$ - E relationships are implemented for the first time to control site-specific growth on NCs. This strategy provides a different way of using seed-mediated NC syntheses to direct selective growth on anisotropic NC seeds by following curvature-selective, facet-selective, and specific exposed facet design rules. Although we only report proof-of-concept architectures of Au, Ag, and Pd here, the strategy presented is generalizable, and more sophisticated architectures with other compositional combinations likely can be synthesized. Given the enormous library of nanostructures that can be tailored by this universal strategy, this work advances the NC design field by allowing for greater structural complexity,

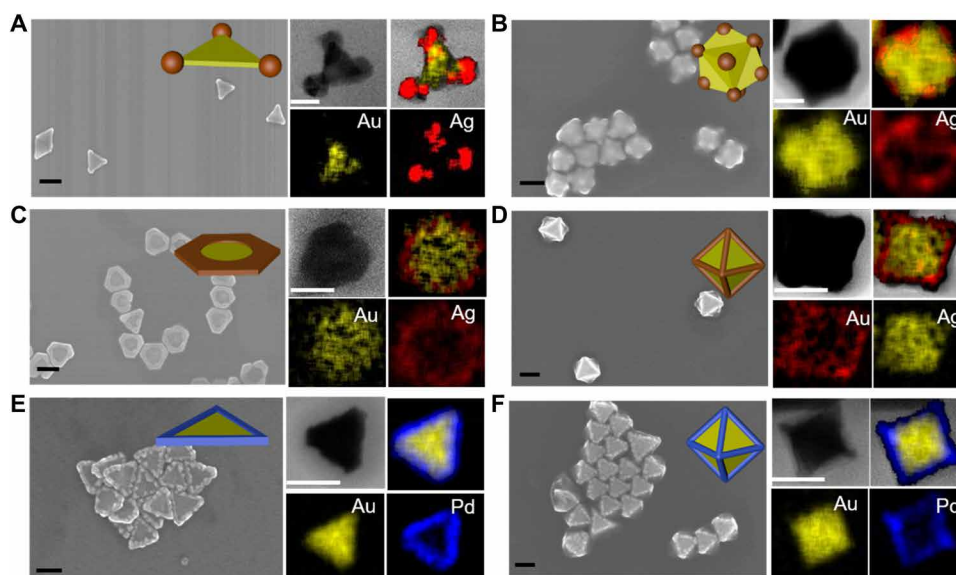


Fig. 5. Growth of multicomponent NCs. SEM images and corresponding elemental maps of the (A and B) corner- and (C and D) edge-selective growth of Ag on Au (A and C) nanoprisms, (B) concave rhombic dodecahedra, and (D) octahedra. SEM images and elemental maps showing the edge-selective growth of Pd on Au (E) nanoprisms and (F) octahedra. For the elemental maps: yellow, Au; red, Ag; and blue, Pd. Scale bars, 100 nm.

specificity, and compositional diversity. Such structures will positively affect a broad range of disciplines, spanning catalysis, plasmonics, magnetics, electronics, biology, and medicine.

MATERIALS AND METHODS

Functionalization of anisotropic NCs

Anisotropic NCs were functionalized with mPEG6 disulfide. One-milliliter aliquots of the as-synthesized NC solution were centrifuged for 6 min at 5000 to 10,000 rpm depending on the NC shape used. After the supernatant was removed, the NCs were resuspended in water and centrifuged a second time under the same centrifugation conditions as the first time. After removal of the supernatant, 900 μ l of 1 μ M mPEG6 disulfide and 100 μ l of 1 weight % (wt %) SDS were added directly to the pellet. The NC solution was placed on a shaker at 1000 rpm for 1 day. To remove excess mPEG6 disulfide, the NC solution was centrifuged three times with the supernatant removed each time, and then the NCs were resuspended in 0.1 wt % SDS after the first two centrifugation steps and in 10 mM CTAB after the third centrifugation step. All the functionalized NCs used as seeds for the following experiments were at a 10 optical density (OD) concentration.

Corner/edge-selective growth

The functionalized NCs were used as seeds for subsequent growth with different AA and CTAB concentrations. Typically, for corner- and edge-selective growth, 6.24 μ l of 25 mM HAuCl₄ was added into 1.25 ml of 10 mM CTAB solution, and then 100 mM AA (for corner-selective growth, 2 to 3 μ l; for edge-selective growth, 10 to 11 μ l depending on different shapes of seeds) was added. The solution was mixed by vortexing for 10 s. Next, 60 μ l of seeds was injected, immediately followed by vortexing for 10 s. After allowing 4 hours for completion of NC growth, the reaction mixture was purified from excess reagents by centrifugation (5 min at 5000 to 10,000 rpm depending on shapes of different seeds). The supernatant was removed, and the NCs were resuspended in 1.0 ml of 1 mM CTAB by brief sonication (~10 s).

Facet-selective growth

For nanorods, 1.25 ml of 10 mM CTAB, 6.24 μ l of 25 mM HAuCl₄, and 15 μ l of 100 mM AA were mixed. Then, 60 μ l of seeds was injected, and the solution was allowed to react for 4 hours. Moreover, for nanodisks, 1.25 ml of 10 mM CTAB, 6.24 μ l of 25 mM HAuCl₄, and 2.5 μ l of 100 mM AA were mixed. Then, 30 μ l of seeds was injected, and the solution was allowed to react for 6 hours.

Exposed facet control

The concentration of CTAB was adjusted to produce site-specifically grown NCs with different types of exposed facets (with the other reaction conditions the same as in the case of the corner/edge-selective growth of NCs). Ten mM CTAB was used to synthesize grown NCs bound by high-energy surfaces, while 100 mM CTAB was used for low-energy surfaces. The amount of deposition was increased by decreasing the amount of seeds from 60 to 6 μ l.

Synthesis of heterogeneous NCs

Synthesis of Au/Ag NCs: 60 μ l of seeds was added to 1.25 ml of 10 mM CTAB solution containing 15.6 μ l of 10 mM AgNO₃. Afterward, 1 M NaOH (for corner selective growth, 7.5 μ l; for edge selective growth, 10 μ l) was introduced. After thorough mixing, 75 μ l of

100 mM AA was finally injected, immediately followed by 10 s of vortexing. The solution was kept at room temperature overnight. NaOH was used here to increase the pH of the growth solution, which decreased the reduction potential of AA and thus increased $\Delta\mu$ of the growth solution.

Synthesis of Au/Pd NCs: 10 mM H₂PdCl₄ aqueous solution was prepared by completely dissolving 89 mg of PdCl₂ in 50 ml of 20 mM HCl in a boiling water bath. A total of 1.25 ml of 10 mM CTAB, 60 μ l of seeds, and 15.6 μ l of 10 mM H₂PdCl₄ were mixed. Then, 15 μ l of 100 mM AA was injected, and the solution was allowed to react overnight.

SUPPLEMENTARY MATERIALS

Supplementary material for this article is available at <http://advances.sciencemag.org/cgi/content/full/7/3/eabf1410/DC1>

REFERENCES AND NOTES

- C. Chen, Y. Kang, Z. Huo, Z. Zhu, W. Huang, H. L. Xin, J. D. Snyder, D. Li, J. A. Herron, M. Mavrikakis, M. Chi, K. L. More, Y. Li, N. M. Markovic, G. A. Somorjai, P. Yang, V. R. Stamenkovic, Highly crystalline multimetallic nanoframes with three-dimensional electrocatalytic surfaces. *Science* **343**, 1339–1343 (2014).
- Q. Fu, W.-X. Li, Y. Yao, H. Liu, H.-Y. Su, M. Ding, X.-K. Gu, L. Chen, Z. Wang, H. Zhang, B. Wang, X. Bao, Interface-confined ferrous centers for catalytic oxidation. *Science* **328**, 1141–1144 (2010).
- J. C. Hill, A. T. Landers, J. A. Switzer, An electrodeposited inhomogeneous metal-insulator-semiconductor junction for efficient photoelectrochemical water oxidation. *Nat. Mater.* **14**, 1150–1155 (2015).
- A. Demortière, R. D. Schaller, T. Li, S. Chattopadhyay, G. Krylova, T. Shibata, P. C. dos Santos Claro, C. E. Rowland, J. T. Miller, R. Cook, B. Lee, E. V. Shevchenko, In situ optical and structural studies on photoluminescence quenching in CdSe/CdS/Au heterostructures. *J. Am. Chem. Soc.* **136**, 2342–2350 (2014).
- M. B. Cortie, A. M. McDonagh, Synthesis and optical properties of hybrid and alloy plasmonic nanoparticles. *Chem. Rev.* **111**, 3713–3735 (2011).
- C. Xu, B. Wang, S. Sun, Dumbbell-like Au–Fe₃O₄ nanoparticles for target-specific platin delivery. *J. Am. Chem. Soc.* **131**, 4216–4217 (2009).
- I. Schick, S. Lorenz, D. Gehrig, A.-M. Schilman, H. Bauer, M. Panthöfer, K. Fischer, D. Strand, F. Laquai, W. Tremel, Multifunctional two-photon active silica-coated Au@MnO janus particles for selective dual functionalization and imaging. *J. Am. Chem. Soc.* **136**, 2473–2483 (2014).
- W. H. Lai, Y. X. Wang, Y. Wang, M. Wu, J. Z. Wang, H. K. Liu, S. L. Chou, J. Chen, S. X. Dou, Morphology tuning of inorganic nanomaterials grown by precipitation through control of electrolytic dissociation and supersaturation. *Nat. Chem.* **11**, 695–701 (2019).
- K. D. Gilroy, A. Ruditskiy, H. C. Peng, D. Qin, Y. Xia, Bimetallic nanocrystals: Syntheses, properties, and applications. *Chem. Rev.* **116**, 10414–10472 (2016).
- Y. Xia, Y. Xiong, B. Lim, S. E. Skrabalak, Shape-controlled synthesis of metal nanocrystals: Simple chemistry meets complex physics? *Angew. Chem. Int. Ed.* **48**, 60–103 (2009).
- C. Burda, X. Chen, R. Narayanan, M. A. El-Sayed, Chemistry and properties of nanocrystals of different shapes. *Chem. Rev.* **105**, 1025–1102 (2005).
- C. Y. Chiu, Y. Li, L. Ruan, X. Ye, C. B. Murray, Y. Huang, Platinum nanocrystals selectively shaped using facet-specific peptide sequences. *Nat. Chem.* **3**, 393–399 (2011).
- Y. Xiong, Y. Xia, Shape-controlled synthesis of metal nanostructures: The case of palladium. *Adv. Mater.* **19**, 3385–3391 (2007).
- M. Chen, B. Wu, J. Yang, N. Zheng, Small adsorbate-assisted shape control of Pd and Pt nanocrystals. *Adv. Mater.* **24**, 862–879 (2012).
- M. N. O'Brien, M. R. Jones, K. A. Brown, C. A. Mirkin, Universal noble metal nanoparticle seeds realized through iterative reductive growth and oxidative dissolution reactions. *J. Am. Chem. Soc.* **136**, 7603–7606 (2014).
- J. Zhang, M. R. Langille, C. A. Mirkin, Photomediated synthesis of silver triangular bipyramids and prisms: The effect of pH and BSPP. *J. Am. Chem. Soc.* **132**, 12502–12510 (2010).
- R. Jin, Y. Cao, C. A. Mirkin, K. L. Kelly, G. C. Schatz, J. G. Zheng, Photoinduced conversion of silver nanospheres to nanoprisms. *Science* **294**, 1901–1903 (2001).
- M. R. Langille, M. L. Personick, J. Zhang, C. A. Mirkin, Defining rules for the shape evolution of gold nanoparticles. *J. Am. Chem. Soc.* **134**, 14542–14554 (2012).
- M. L. Personick, M. R. Langille, J. Zhang, N. Harris, G. C. Schatz, C. A. Mirkin, Synthesis and isolation of (110)-faceted gold bipyramids and rhombic dodecahedra. *J. Am. Chem. Soc.* **133**, 6170–6173 (2011).

20. M. L. Personick, M. R. Langille, J. Zhang, C. A. Mirkin, Shape control of gold nanoparticles by silver underpotential deposition. *Nano Lett.* **11**, 3394–3398 (2011).
21. J. Zhang, M. R. Langille, M. L. Personick, K. Zhang, S. Li, C. A. Mirkin, Concave cubic gold nanocrystals with high-index facets. *J. Am. Chem. Soc.* **132**, 14012–14014 (2010).
22. C. R. Laramy, H. Lopez-Rios, M. N. O'Brien, M. Girard, R. J. Stawicki, B. Lee, M. O. De La Cruz, C. A. Mirkin, Controlled symmetry breaking in colloidal crystal engineering with DNA. *ACS Nano* **13**, 1412–1420 (2019).
23. Y. C. Tsao, S. Rej, C. Y. Chiu, M. H. Huang, Aqueous phase synthesis of Au-Ag core-shell nanocrystals with tunable shapes and their optical and catalytic properties. *J. Am. Chem. Soc.* **136**, 396–404 (2013).
24. F. Wang, S. Cheng, Z. Bao, J. Wang, Anisotropic overgrowth of metal heterostructures induced by a site-selective silica coating. *Angew. Chem. Int. Ed.* **52**, 10344–10348 (2013).
25. S. Ham, H.-J. Jang, Y. Song, K. L. Shuford, S. Park, Octahedral and cubic gold nanoframes with platinum framework. *Angew. Chem. Int. Ed.* **54**, 9025–9028 (2015).
26. Y. Yu, Q. Zhang, J. Xie, J. Y. Lee, Engineering the architectural diversity of heterogeneous metallic nanocrystals. *Nat. Commun.* **4**, 1454 (2013).
27. D. A. Walker, E. K. Leitsch, R. J. Nap, I. Szeleifer, B. A. Grzybowski, Geometric curvature controls the chemical patchiness and self-assembly of nanoparticles. *Nat. Nanotechnol.* **8**, 676–681 (2013).
28. M. Wu, A. M. Vartanian, G. Chong, A. K. Pandiakumar, R. J. Hamers, R. Hernandez, C. J. Murphy, Solution NMR analysis of ligand environment in quaternary ammonium-terminated self-assembled monolayers on gold nanoparticles: The effect of surface curvature and ligand structure. *J. Am. Chem. Soc.* **141**, 4316–4327 (2019).
29. Z. Wang, G. Yang, Z. Zhang, M. Jin, Y. Yin, Selectivity on etching: Creation of high-energy facets on copper nanocrystals for CO₂ electrochemical reduction. *ACS Nano* **10**, 4559–4564 (2016).
30. I. V. Markov, *Crystal Growth for Beginners* (World Scientific, 2003).
31. B. E. Janicek, J. G. Hinman, J. J. Hinman, S. h. Bae, M. Wu, J. Turner, H.-H. Chang, E. Park, R. Lawless, K. S. Suslick, C. J. Murphy, P. Y. Huang, Quantitative imaging of organic ligand density on anisotropic inorganic nanocrystals. *Nano Lett.* **19**, 6308–6314 (2019).
32. H. X. Lin, Z. C. Lei, Z. Y. Jiang, C. P. Hou, D. Y. Liu, M. M. Xu, Z. Q. Tian, Z. X. Xie, Supersaturation-dependent surface structure evolution: From ionic, molecular to metallic micro/nanocrystals. *J. Am. Chem. Soc.* **135**, 9311–9314 (2013).
33. J. Y. Kim, M. G. Han, M. Bin Lien, S. Magonov, Y. Zhu, H. George, T. B. Norris, N. A. Kotov, Dipole-like electrostatic asymmetry of gold nanorods. *Sci. Adv.* **4**, e1700682 (2018).
34. J. E. Millstone, S. J. Hurst, G. S. Métraux, J. I. Cutler, C. A. Mirkin, Colloidal gold and silver triangular nanoprisms. *Small* **5**, 646–664 (2009).
35. J. E. Millstone, W. Wei, M. R. Jones, H. Yoo, C. A. Mirkin, Iodide ions control seed-mediated growth of anisotropic gold nanoparticles. *Nano Lett.* **8**, 2526–2529 (2008).
36. K. L. Young, M. R. Jones, J. Zhang, R. J. Macfarlane, R. Esquivel-Sirvent, R. J. Nap, J. Wu, G. C. Schatz, B. Lee, C. A. Mirkin, Assembly of reconfigurable one-dimensional colloidal superlattices due to a synergy of fundamental nanoscale forces. *Proc. Natl. Acad. Sci. U.S.A.* **109**, 2240–2245 (2012).
37. J. Rodríguez-Fernández, J. Pérez-Juste, P. Mulvaney, L. M. Liz-Marzán, Spatially-directed oxidation of gold nanoparticles by Au(III)–CTAB complexes. *J. Phys. Chem. B* **109**, 14257–14261 (2005).
38. M. N. O'Brien, M. R. Jones, K. L. Kohlstedt, G. C. Schatz, C. A. Mirkin, Uniform circular disks with synthetically tailorable diameters: Two-dimensional nanoparticles for plasmonics. *Nano Lett.* **15**, 1012–1017 (2015).
39. X. Ye, C. Zheng, J. Chen, Y. Gao, C. B. Murray, Using binary surfactant mixtures to simultaneously improve the dimensional tunability and monodispersity in the seeded growth of gold nanorods. *Nano Lett.* **13**, 765–771 (2013).
40. A. Sánchez-Iglesias, N. Winckelmans, T. Altantzis, S. Bals, M. Grzelczak, L. M. Liz-Marzán, High-yield seeded growth of monodisperse pentatwinned gold nanoparticles through thermally induced seed twinning. *J. Am. Chem. Soc.* **139**, 107–110 (2017).
41. Q. Zeng, S. Xu, Thermodynamics and characteristics of heterogeneous nucleation on fractal surfaces. *J. Phys. Chem. C* **119**, 27426–27433 (2015).

Acknowledgments: We acknowledge K. Gibson [Northwestern University (NU)], S. M. Rupich (NU), and S. H. Petrosko (NU) for providing editorial input. **Funding:** This material is based upon work supported by the Air Force Office of Scientific Research award FA9550-17-1-0348 (nanoparticle synthesis); the Center for Bio-Inspired Energy Science, an Energy Frontier Research Center funded by the U.S. Department of Energy, Office of Science, Basic Energy Sciences under award DE-SC0000989 (SEM characterization); the Vannevar Bush Faculty Fellowship program sponsored by the Basic Research Office of the Assistant Secretary of Defense for Research and Engineering and funded by the Office of Naval Research through grant N00014-15-1-0043 (TEM characterization); and the Sherman Fairchild Foundation Inc. (ligand functionalization). This work made use of the EPIC facility of Northwestern University's NUANCE Center, which has received support from the Soft and Hybrid Nanotechnology Experimental (SHyNE) Resource (NSF ECCS-1542205); the MRSEC program (NSF DMR-1720139) at the Materials Research Center; the International Institute for Nanotechnology (IIN); the Keck Foundation; and the State of Illinois, through the IIN. **Author contributions:** Y.L., W.Z., and H.L. performed the experiments. C.A.M. supervised the project, and all authors analyzed the data and helped in interpretation. Y.L., W.Z., H.L., L.S., D.S., and C.A.M. all contributed to the writing of the manuscript. **Competing interests:** C.A.M., Y.L., H.L., and W.Z. are inventors on a U.S. patent application filed on this work. The authors declare that they have no other competing interests. **Data and materials availability:** All data needed to evaluate the conclusions in the paper are present in the paper and/or the Supplementary Materials. Additional data related to this paper may be requested from the authors.

Submitted 6 October 2020
Accepted 24 November 2020
Published 15 January 2021
10.1126/sciadv.abf1410

Citation: Y. Li, H. Lin, W. Zhou, L. Sun, D. Samanta, C. A. Mirkin, Corner-, edge-, and facet-controlled growth of nanocrystals. *Sci. Adv.* **7**, eabf1410 (2021).